

Particle image velocimetry of non-axisymmetric stenosis models

C.S. Chua^{1,2}, G.J. Sheard^{1,2}, S. Dubsy^{1,2}, S. Higgins^{1,2}, R.A. Jamison¹, A. Fouras^{1,2} and K. Hourigan^{1,2}

¹Division of Biological Engineering, Faculty of Engineering, Monash University, VIC 3800, Australia.
Fouras@eng.monash.edu

²Fluids Laboratory for Aeronautical & Industrial Research, Department of Mechanical & Aerospace Engineering, Monash University, VIC 3800, Australia.

ABSTRACT

Steady flow through straight tubes featuring non-axisymmetric sinusoidal constrictions of area reduction 50%, are used as simplified models of stenosed human arteries. Numerically, a spectral element code is utilized to investigate physiological flow characteristics; showing the development of recirculation regions, as well as high and low wall shear stress (WSS) with increasing Reynolds number (Re) and degree of stenosis asymmetry. The non-axisymmetric stenosis geometries are further used to develop a single camera particle image velocimetry (PIV) technique for *in vitro* cardiovascular models, whereby the instantaneous three-dimensional velocity vector field and shear stress distribution are measured.

1. INTRODUCTION

The study of flows in straight tubes featuring smooth sinusoidal constrictions are of great interest as they serve as idealised models of human arterial occlusions (stenoses). Arterial disease is the leading cause of death in the developed world [1], yet limited research has been conducted into fully three-dimensional vessel constriction geometries that are biased to one side of the arterial wall. The observation that stenoses are rarely axisymmetric in practice (see Figure 1), motivates the study of arterial fluid mechanics through non-axisymmetric models, and stands to contribute significantly to medical research.

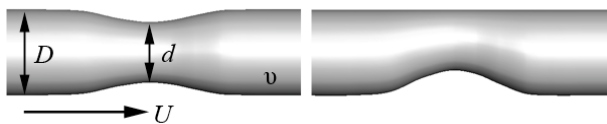


Figure 1. Models comparing the stenosed region of axisymmetric (left) and non-axisymmetric (right) geometries that feature an area reduction of 50%.

Research into stenoses haemodynamics has accelerated in the field of engineering due to the increasingly powerful use of computational fluid dynamics (CFD). Much of the focus has been concentrated to axisymmetric three-dimensional geometries such as exhibited in Blackburn and Sherwin [1], and Griffith *et al.* [8]. Constricted flows between flat plates [7], experimental flow visualization within stenosed cylinders [8] and pressure measurements of simple *in vitro* models [3] have also been conducted to analyze the effects of stenosis geometry, noting increased effects with non-axisymmetry. Chua *et al.* [2] performed a numerical study on stenosis geometry, finding that dissipation of the shear layers associated with downstream recirculation occurred more quickly with axisymmetric stenoses. Furthermore, increasingly non-axisymmetric geometries produced an increase in vorticity perpendicular to the constriction, increases in

recirculation regions, as well as the development of higher and lower WSS in the vicinity and downstream of the throat.

PIV is a well-established, non-intrusive optical method for the instantaneous measurement of fluid velocity. It offers higher resolution than other imaging techniques such as MRI and ultrasound [5], making PIV a favourable, emerging technique for visualizing cardiovascular flows. Traditional PIV sees the use of a thin laser sheet to provide a two-dimensional, two-component vector field of the flow – suitable for axisymmetric geometries. However, complex flows through non-axisymmetric stenosis models need fully three-dimensional data acquisition through the interrogated volume. Tomographic PIV is a technique [4] used to reconstruct the three-dimensional velocity vector field in a volume. Similarly, the current study develops a high spatial and temporal resolution, PIV technique that uses volume illumination by coherent laser light to illuminate tracer particles within the transparent blood analogue, and achieves this through the use of a single camera. This proves advantageous over other currently utilized PIV variations: Stereo-PIV, where multiple cameras are used to determine three components of velocity; holographic-PIV, where the particle displacements are acquired holographically to allow determination of three components of velocity; and digital inline holography which offers low resolution, three-dimensional particle tracking [5].

The emphasis of the present work is to investigate the flow through three-dimensional non-axisymmetric constriction geometries, both numerically and experimentally. The CFD study will extend the work of Chua *et al.* [2] to higher resolution. The development of the PIV technique will offer data from the first implementation of PIV using physiologically relevant flows through cardiovascular disease models. The scope of the technique will lend itself to validation with the numerical data into the future, and to easily allow the use of different inflow profiles and frequencies across a range of physiological blood flow velocities.

Changes in fluid flow velocity through the stenosed region are of particular interest as it lends itself to the development of flow stagnation, as well as increased and decreased WSS compared with that exhibited by a non-stenosed artery. High WSS is indicative of endothelial cell damage, platelet activation and plaque rupture, whereas low WSS is commonly associated with atherosclerotic plaque formation [12].

2. PROBLEM DEFINITION & METHODOLOGY

We consider flows using a Newtonian rheology assumption and kinematic viscosity ν , in a rigid straight tube of diameter D , featuring smooth sinusoidal constrictions that are given an arbitrary length scale of $L = 2D$ (see Figure 1). Four geometries were utilised, consisting of a *straight pipe*

containing no stenosis, an *axisymmetric* stenosis, a *moderate* stenosis (offset halfway to the pipe wall), and a *severe* stenosis (offset against the pipe wall). All stenoses featured an area reduction of 50% from the pipe diameter. The Reynolds number was defined as $Re = UD/\nu$, where D is the major pipe diameter, U is the fluid velocity, and ν is the kinematic viscosity of blood. Branching and other curvature aspects of real blood vessels were neglected to isolate flow disturbance due to the constriction. A uniform flow profile was input upstream, and the vessel was assumed rigid and impermeable, consistent with previous studies such as Blackburn and Sherwin [1].

2.1 Numerical method

The stenosis was located $4D$ downstream of the inlet, and the domain extended $9D$ past the stenosis to permit downstream flows to be resolved, consistent with Chua *et al.* [2]. An incompressible and unsteady Navier-Stokes solver was employed for the CFD study; validated by Sheard *et al.* [13]. The code utilised a spectral element method for spatial discretization, using high-order polynomial functions to approximate the flow solution within each element [10]. Meshes for all geometries yielded 784 macro elements, with higher element density in the vicinity of the stenosis as well as near the walls. Varying the spectral element polynomial order allowed spatial refinement of the model within each macro element without modifying the base mesh.

The boundary conditions imposed in the numerical study were as follows:

1. Constant reference pressure at the outlet
2. Parabolic Poiseuille flow profile at the inlet
3. Wall is rigid and impermeable
4. Zero velocity at the walls
5. Standard zero normal velocity gradient at the outlet

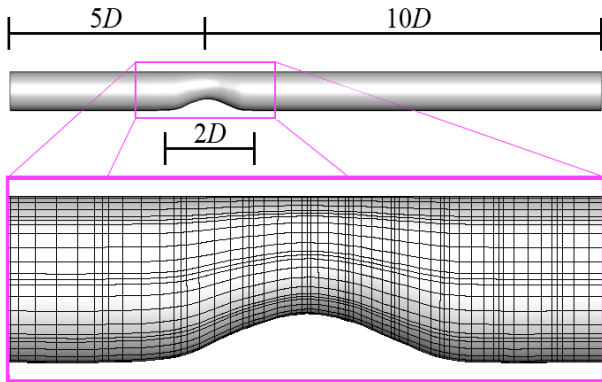


Figure 2. The *severe* geometry's full computational domain, showing spectral elements at the stenosed region for $N = 7$.

The L_2 norm defined as $L_2 = \int_{\Omega} |U| d\Omega$ where U is the velocity vector field, and Ω is the computational domain, was monitored for spatial convergence on the severe stenosis geometry at $Re = 100$ through spectral element polynomial orders up to $N = 10$. The polynomial order was limited by computational power and resources; the $N = 10$ run utilised 23 GB of RAM, taking ~ 25 s to complete one time step, and converged over approximately two weeks of physical computing time. The L_2 calculated with polynomial order $N = 7$ was within 0.01% of the value calculated from the highest polynomial order case, thus all reported values hereafter were computed with $N = 7$.

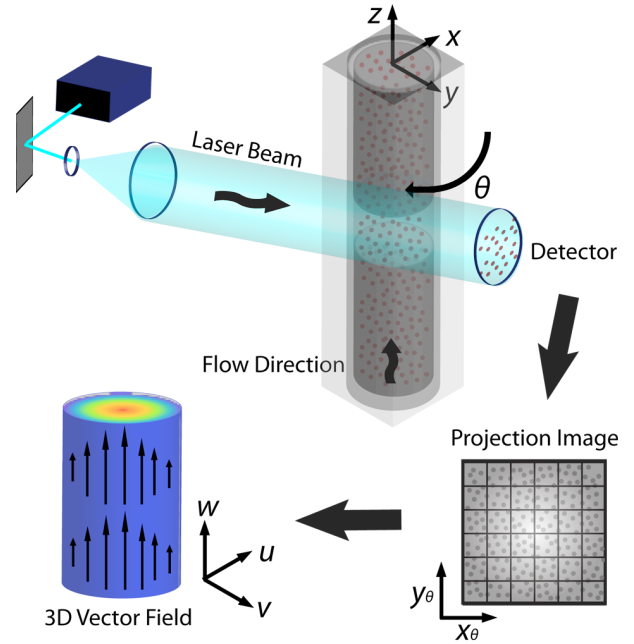


Figure 3. Simple schematic of the experimental method: The particle shadowgraph pairs are captured by the CCD as projection images that are analysed through cross-correlation algorithms to produce a vector field of the volume.

2.2 Experimental method

An experimental rig was constructed to implement the PIV technique. A brief description of the rig is presented here, although a more detailed description is available in [9]. The models were constructed out of transparent acrylic with an inner diameter of $D = 14$ mm, $15D$ total length, and the constriction located $5D$ downstream of the inlet. This provided a fully developed Poiseuille flow entering the constriction and restricted any end effects. The cylindrical models were filled with a fluid mixture of 91% diethyl phthalate (DEP) and 9% ethanol – refractive index matched to the acrylic ($n = 1.49$) at $T_{lab} = 291$ K, with kinematic viscosity recorded at $\nu = 6.7 \times 10^{-6} \text{ m}^2 \text{ s}^{-1}$. The DEP-ethanol mixture presented itself as the best candidate for cardiovascular *in vitro* models due to its high index of refraction and low viscosity [11]. The working fluid mixture was seeded with $\leq 10 \mu\text{m}$ glass spheres at a 1:2000 w/v preparation and pumped through the model internally. This volume of fluid was illuminated in the model using a $30\times$ expanded beam output from a 50 mW diode-pumped solid-state laser at a frequency of 488 nm. The image pairs are then processed using correlation software developed by Fouras [6] to form a three-dimensional velocity vector field of the interrogated flow volume.

3. RESULTS

3.1 Numerical simulations

Figure 5 plots contours of axial velocity obtained from numerical simulations through the plane of stenosis asymmetry. Subfigure (a) represents a healthy, non-stenosed artery exhibiting a uniform parabolic flow profile. Comparing subfigures (a) through (d), all at $Re = 100$, similar level higher and lower axial velocity gradients are exhibited from the *straight pipe* case. This is caused by the increase in flow through the constriction, followed then by a decrease at the

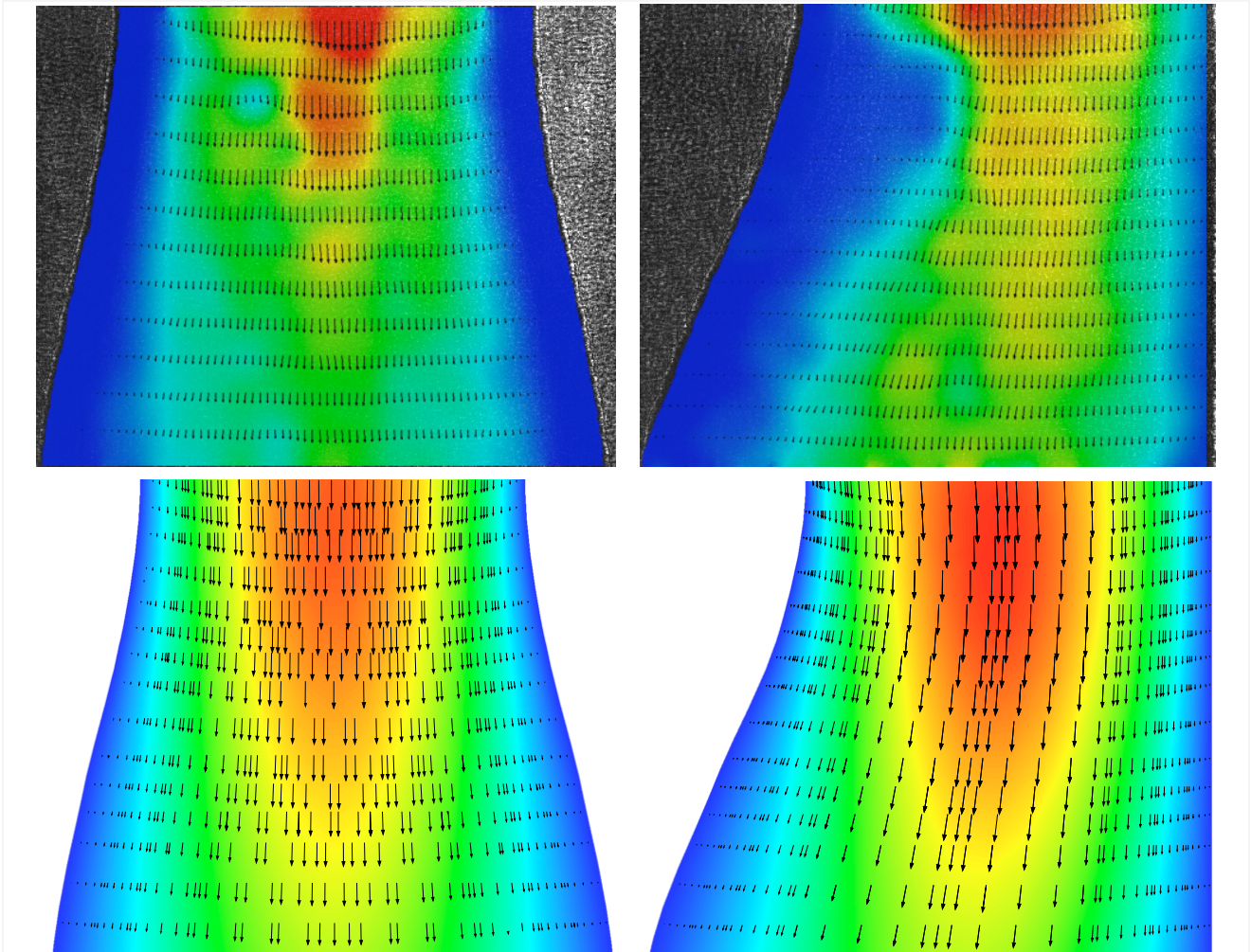


Figure 4. Comparison of PIV with raw image acquisitions behind (top), and CFD output (bottom) for $Re = 10$ exhibiting contours of velocity magnitude overlaid with corresponding vectors, for orthogonal views of the *severe* geometry showing $0.8D$ downstream of the stenosis throat. Contour gradients are shown between $u = 0$ and $3.77\bar{U}$.

walls caused by the area divergence after the throat – indicative of higher than normal WSS at the throat, and lower than normal WSS downstream of the throat, signified by the contours not present in (a). Furthermore, the stagnated flow increases with non-axisymmetry causing stagnated flow to develop in (c), and more prominently noticed as a recirculation region in (d). Further still, with increasing Re of the *severe* geometry, (d) through (f); the recirculation region becomes fully developed and the associated shear layer is seen to extend further downstream with an increase in Reynolds number, denoted by the continuous rapid vertical change in contour gradients. Dissipation of the shear layers occurs quickly for the *axisymmetric* geometry (b).

3.2 PIV of stenosis model

Upon construction and implementation of our experimental rig, a Reynolds number of $Re = 10$ was chosen for the fluid flow, based on the main diameter of the models, $D = 14$ mm, useable pump speed, and the achievable CCD frame rate. A laminar regime also denotes a predictable flow, useful for experimental validation at this stage of proceedings.

Figure 4 (top) shows two orthogonal projections of flow captured through the *severe* geometry, where the raw image acquisitions have been placed behind the PIV volumetric

velocity vector field. The corresponding numerical results (below) show good congruency with the experimental data. High velocity flow is seen through the centre of the throat and a parabolic flow profile trend is seen from the experimental work. Also evident (top) is the emergence of a Womersley flow profile, indicative of slight pulsatility from the working fluid pump's operation.

4. DISCUSSION

Two projections of the three-dimensional PIV technique have been captured and shown in this paper, showing our single camera, PIV technique has been successfully implemented, noted in particular by the capture of a Womersley flow profile. The next stage of the technique implementation is to capture further projections of the flow, in order to form a fully three-dimensional velocity vector field of the fluid volume. From here, input parameters such as Reynolds number may then be altered to recreate the recirculation regions and WSS changes as shown by the numerical work in Figure 5, in order to validate the technique. With the use of the experimental rig, pulsatile inflow can be input and studied, offering significant advantage over the equivalent, fully three-dimensional CFD analysis, which is computationally exhaustive.

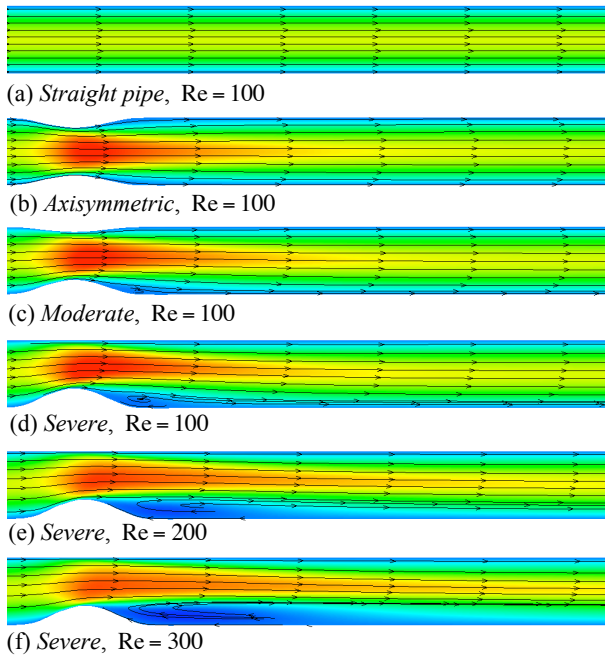


Figure 5. Axial velocity of the flow overlaid with corresponding streamtraces from the CFD simulations, comparing all four geometries at $Re=100$, and the *severe* geometry at $Re=100, 200, 300$. Continuous contour gradients are shown between $u = -0.35\bar{U}$ and $3.00\bar{U}$ through a length of $1D$ upstream to $8D$ downstream of the throat.

5. CONCLUSIONS

A three-dimensional PIV technique has been demonstrated to provide a volumetric velocity vector field of flow through a non-axisymmetric stenosis model, using single-source volume illumination with one camera. The subsequent output shows good agreement with the corresponding CFD analysis for a 50% area reduction, *severe* stenosis geometry at $Re = 10$. The numerical study found recirculation zones developing with increasing stenosis asymmetry as well as with an increase in Reynolds number. Furthermore, levels of WSS increase, and shear layer dissipation decreases with these parameters. The numerical findings present useful benchmarks to be cross-referenced from the full implementation of the three-dimensional PIV technique.

The research presented in this paper forms the basis for continuing work encompassing the comparison of axisymmetric and non-axisymmetric stenoses models at a constant area reduction. Full implementation of the three-dimensional PIV technique is underway. Currently under investigation is the effect of steady and pulsatile inflow profiles, at a number of physiologically relevant frequencies, and through a range of physiologically relevant Reynolds numbers that will transition into the turbulent regime, which is dominated by three-dimensional artefacts in the flow such as vortex shedding. The aim will be to capture the onset of such artefacts.

Acknowledgements

The authors gratefully acknowledge financial support from the Australian Research Council under Discovery Grant DP0877327.

REFERENCES

- [1] Blackburn, H.M. & Sherwin, S.J. (2005) Three-dimensional instabilities and transition of steady and pulsatile axisymmetric stenotic flows. *Journal of Fluid Mechanics*, **533**, 297-327.
- [2] Chua, C.S., Sheard, G.J., Ryan, K. & Fouras, A. (2009) Changes in flow and wall shear stresses through arterial constrictions offset from the vessel centre, *ANZIAM Journal*, Vol. 50, C744-C759.
- [3] Dodds, S.R. (2002) The haemodynamics of asymmetric stenoses. *European Journal of Vascular and Endovascular Surgery*, **24**, 332-337.
- [4] Elsinga, G.E., Scarano, F., Wieneke, B. & van Oudheusden, B.W. (2006) Tomographic particle image velocimetry. *Experiments in Fluids*, **41**(6), 933-947.
- [5] Fouras, A., Kitchen, M.J., Dubsky, S., Lewis, R.A., Hooper, S.B. and Hourigan, K. (2009) The past, present, and future of x-ray technology for *in vivo* imaging of function and form. *Journal of Applied Physics*, **105**, 102009.
- [6] Fouras, A., Lo Jacono, D. & Hourigan, K. (2008) Target-free Stereo PIV: a novel technique with inherent error estimation and improved accuracy. *Experiments in Fluids*, **44**(2), 317-329.
- [7] Griffith, M.D., Hourigan, K. & Thompson, M.C. (2004) Numerically modeling blockage effects on the flow between flat plates. In *Proceedings of the 15th Australasian Fluid Mechanics Conference*, Sydney, Australia, 13-17 December.
- [8] Griffith, M.D., Leweke, T., Thompson, M.C. & Hourigan, K. (2009) Pulsatile flow in stenotic geometries: flow behaviour and stability. *Journal of Fluid Mechanics*, **622**, 291-320.
- [9] Higgins, S., Fouras, A. & Hourigan, K. (2009) Image Velocimetry of Optical Projection Tomography Data. In *Proceedings of the 8th International Symposium on Particle Image Velocimetry*, Melbourne, Australia, 25-28 August.
- [10] Karniadakis, G.E. & Sherwin, S.J. (2005) *Spectral/hp Element Methods for CFD*, 2nd ed., Oxford University Press, Oxford.
- [11] Miller, P., Danielson, K., Moody, G., Slifka, A., Drexler, E. & Hertzberg, J. (2006) Matching index of refraction using a diethyl phthalate/ethanol solution for *in vitro* cardiovascular models, *Experiments in Fluids*, **41**(3), 375-381.
- [12] Nesbitt, W.S., Westein, E., Lopez, F.J.T., Tolouei, E., Mitchell, A., Fu, J., Carberry, J., Fouras, A. & Jackson, S.P. (2009) Identification of a New Rheology Dependent Platelet Aggregation Mechanism Driving Thrombus Growth. *Nature Medicine*, in press.
- [13] Sheard, G.J. & Ryan, K. (2007) Pressure-driven flow past spheres moving in a circular tube. *Journal of Fluid Mechanics*, **592**, 233-262.